Low-temperature ohmic contacts to n-ZnSe for all-electrical quantum devices

Johanna Janßen,[*,†] Felix Hartz,[‡] Till Huckemann,[‡] Christian Kamphausen,[‡] Malte Neul,[‡] Lars R. Schreiber,[‡] and Alexander Pawlis[*,†]

†*Peter Grünberg Institute 9 and JARA - FIT, Forschungszentrum Jülich GmbH, Germany*

‡*JARA - Institute for Quantum Information, RWTH Aachen University, Germany*

E-mail: jo.janssen@fz-juelich.de; a.pawlis@fz-juelich.de

Abstract

The II/VI semiconductor ZnSe is an ideal host for novel devices for quantum computation and communication as it can be made nuclear-spin free to obtain long electron spin coherence times, exhibits no electron valley-degeneracy and allows optical access. Prerequisite to electrical quantum devices are low-resistive ohmic-contacts operating at temperatures below 10 K, which have not been achieved in ZnSe, yet. Here, we present a comprehensive study on the realization of ohmic contacts to ZnSe by three different technological approaches, ion implantation of halogene donors, epitaxial doping with *in-situ* contact processing, and finally, a unique ZnSe regrowth technique. The latter allows to fabricate ohmic contacts with local doping that can be used to connect to a buried conducting channel such as used in unipolar devices. DC measurements at cryogenic temperature revealed high contact resistivity for ohmic contacts to ZnSe doped via halogene ion implantation, while in-situ Aluminium (Al) contacts on epitaxially Chlorine-doped ZnSe yield record low contact resistivities in the order of $10^{-5}\,\Omega\mathrm{cm}^2$ at 4 K. Finally, making use of the regrowth technique, local ohmic contacts to ZnSe are

demonstrated, which still feature low contact resistivities of $(1.4 \pm 0.4) \times 10^{-3}\,\Omega\mathrm{cm}^2$ at 4 K. These findings pave the way for new electrical devices in the ZnSe material system such as field effect transistors, electrostatically defined qubits or quantum repeaters operating at cryogenic temperature.

Introduction

Generally, low-temperature ohmic contacts to n-type classic II/VI semiconductors (Zn, Mg, Cd, -sulfides, -selenides and -tellurides) are an unexplored field with sparse results so far. Most of the suitable metals lead already at room temperature (RT) to considerable high contact resistances: For example in n-type ZnTe several metals (Al, Mg, W, InHg) were studied in Ref. 1 and the best performance was found for tungsten contacts yielding contact resistivities of about $4 \times 10^{-2}\,\Omega\mathrm{cm}^2$. For n-type CdTe slightly lower resistivities of about $1 - 2 \times 10^{-2}\,\Omega\mathrm{cm}^2$ were achieved with in-diffused In contacts.[2] Substantially higher contact resistivities of about $1 - 5 \times 10^{-1}\,\Omega\mathrm{cm}^2$ are reported for ZnS using Indium alloyed with different metals.[3] Similarly, most of the suitable metals for ZnSe also lead to considerably high contact resistances exceeding $1 \times 10^{-2}\,\Omega\mathrm{cm}^2$ (for In and Mg contacts[4]) and poorly linear current/voltage characteristics at low operating voltages. The lowest room temperature contact resistance ($3.4 \times 10^{-4}\,\Omega\mathrm{cm}^2$) has been observed with annealed Ti/Pt/Au contacts on highly Cl-doped ($2 \times 10^{19}\,\mathrm{cm}^{-3}$) n-type ZnSe.[5] In Refs. 6,7, successful ohmic contacts to a buried 2-dimensional electron gas in manganese doped ZnSe/(Cd,Mn)Se heterostructures and superlattices was demonstrated by in-diffusion of Indium into the ZnSe. But in all these studies no quantitative analysis of the contact performance especially at cryogenic temperature is reported.

The absence of scalable and locally doped ohmic contacts operating at 4 K, currently hamper the exploit of the excellent properties of ZnSe and related materials concerning quantum systems such as spin qubit devices[8,9] and quantum repeaters required for quantum computing and quantum communication, respectively. ZnSe is the ideal host crystal for

these applications for the following six reasons: (1) It is a direct semiconductor providing efficient radiative recombination due to large transition matrix elements in the material. Towards a spin-to-photon interface,[10–13] initialization and read-out of a single electron spin by a single photon carrying the spin correlated frequency and polarization state has been recently demonstrated.[14] (2) ZnSe can be isotopically purified towards zero nuclear spin[15,16] to reduce hyperfine interaction and by that, to extend the single-spin dephasing time. (3) ZnSe/(Zn,Mg)Se heterostructures facilitate a planar gate architecture and therefore are compatible with surface-code quantum error correction.[17] (4) As the lattice parameters of GaAs and ZnSe only differ by 0.2 %, high quality ZnSe/(Zn,Mg)Se heterostructures with defect densities as low as that of GaAs/(Al,Ga)As can be grown by molecular beam epitaxy (MBE).[18] (5) The effective electron mass of ZnSe (e.g. $0.145\,m_\mathrm{e}$[19]) is small and fabrication of electrostatically defined quantum dots (EDQDs) is not limited by the pitch of current gating technology.[20] (6) Finally, ZnSe exhibits no valley degeneracy and operation at elevated temperatures up to 1 K might not be hampered by insufficient valley splitting.[21]

To leverage the advantages of the ZnSe/(Zn,Mg)Se system for quantum device applications, we aim at locally doped ohmic contacts with linear current/voltage characteristics and reproducible contact resistances of less than 1×10^{-2} $\Omega\mathrm{cm}^2$ operating at typical biasing below 1 mV and at 4 K. This will allow for ohmic contact resistances smaller than the typical resistance of a quantum point contact (order of von Klitzing constant $R_\mathrm{K} \approx 26$ kΩ) or a single electron transistor at a bias, which is smaller than the typical charging energy of an electrostatically defined quantum dot.[8,9,22] Also the impact due to Johnson noise generated at the contact resistance is sufficiently low for spin qubit devices[23] and ohmic heat dissipation compared to the typical cooling power of mixing cryostat at 100 mK is neglegible. For ZnSe and related materials, n-type doping is usually performed by Chlorine (Cl) which efficiently substitutes Se atoms in the lattice due to similar atomic radii of both species. To date, typical bulk mobilities of $150-530$ $\mathrm{cm}^2(\mathrm{Vs})^{-1}$ and free carrier densities up to 10^{19} cm^{-3} can be achieved at room temperature (RT).[24,25] The latter is sufficiently high to exceed the

metal-insulator-transition (MIT) in ZnSe,[24] i.e. to maintain sufficient conductivity also at cryogenic temperature. Typically, the contact resistance can be reduced by in-diffusion of the ohmic metals in a post-metallization annealing procedure. In ZnSe, this approach is counterproductive, as this can lead to disordering related generation and diffusion of group-II vacancies[26] to the ZnSe surface. Laks et al.[27] reported that Zn-vacancies form complexes with p-type conductivity in ZnSe. Together with the efficient thermally induced diffusion these defects likely can compensate the n-type conductivity below the ohmic contacts. This might lead to the formation of additional barriers and nonlinearities of the current/voltage characteristics. Apart from further improvement of the contact performance, the ability of deterministically defined, spatially localized doping below the ohmic contacts must be demonstrated to pave the way towards realization of EDQDs in ZnSe.

In this report, we address both open issues of ohmic contacts to n-type ZnSe, the paper is organized as follows: In the first section we will compare conductivity of n-type ZnSe obtained via implantation of Fluorine (F) and Cl and alternatively, by epitaxial doping of ZnSe during the MBE growth. Especially *in-situ* doping with $ZnCl_2$ has been intensively studied and allows to achieve free carrier densities up to 10^{19} cm^{-3} reported in Refs. 25,28. But this approach cannot be directly applied for selective doping of ZnSe below the ohmic contacts. Moreover, we observe that ion implantation technique, typically used for local doping of high-quality Si qubits, is not applicable to ZnSe as the ion bombardment increases the Zn-vacancy concentration. In the second section we report on the properties of different ohmic contact metals deposited by *in-situ* (ZnSe kept in ultrahigh vacuum (UHV)) method on ZnSe doped with Cl during MBE growth (in the following ZnSe:Cl) at RT and 4 K. Especially the *in-situ* deposition is a promising improvement as this avoids the formation of an additional oxide layer between ZnSe and metal. Finally, in the last section of the paper, we demonstrate a scalable approach of spatially selective n-type doping of ZnSe based on a sophisticated regrowth technique of ZnSe:Cl by MBE in combination with the optimized *in-situ* ohmic contacts.

Fabrication Methods

The samples consist of ZnSe layers with thicknesses of $t = 700 - 1100\,\mathrm{nm}$ grown by MBE on undoped GaAs substrates. The ZnSe was doped *in-situ* with Cl during the epitaxial growth or undoped (typical n-type background carrier concentration of $\sim 10^{15}\,\mathrm{cm}^{-3}$). The latter was used for the investigation of doping via ion implantation with F or Cl at different acceleration voltages and ion doses (see Tab. 1). All implantation runs were performed under an angle of 7° with respect to the MBE growth axis in (100)-direction.

Metal deposition was accomplished directly after the MBE growth of ZnSe. For this *in-situ* deposition, the samples were kept under UHV conditions during the whole process to suppress the formation of an oxide layer at the ZnSe/metal interface. The implanted samples were *in-situ* covered with about 50 nm thick Al contact layers. In case of the samples doped during growth, we tested the *in-situ* technique with different metals (Al, Ti, Mg) using typical contact layer thickness of about 120-150 nm. For the Mg contacts the thickness was 20 nm below a 100 nm thick Al passivation layer.

Unless otherwise specified, we have chosen the transmission line model (TLM)[29] contact geometry to evaluate both, the contact and the bulk resistance in our n-ZnSe samples. Contact patterns were defined by optical lithography using the photoresist AZ 5214 E in a positive process and the developer AZ 326 MIF. After resist patterning the metal was etched either by TMAH based developer for Al contacts, or HF (1%) for Mg or Ti contacts. The size of the contact pads is typically $190\,\mu\mathrm{m} \times 75\,\mu\mathrm{m}$. For the TLM design the contact spacing ranges from 30 µm to 180 µm in steps of 30 µm. For several exemplary samples, mesa structures with channel widths of 10 µm and 50 µm were fabricated by repeating the positive resist lithography process and applying a subsequent etching of the ZnSe down to the GaAs substrate with a $K_2Cr_2O_7 : HBr : H_2O$ solution.

In order to determine the doping concentration in the ZnSe samples, secondary ion mass spectrometry (SIMS) analyses were performed. The background-corrected intensity profiles were quantified using an implantation reference sample. The free-carrier concentration in

the ZnSe samples doped *in-situ* during growth was extracted from Hall measurements with the van der Pauw method.

Results and Discussion

Ohmic contacts to Fluorine and Chlorine implanted ZnSe

The contact resistance of ohmic contacts to semiconductors can be substantially reduced by the local enhancement of the free-carrier concentration in the semiconductor below the contact metal. In various material systems,[30–32] efficient local doping was achieved by ion implantation. Since the halogenides are prominent n-type dopants for II/VI semiconductors (Ref. 33 and references therein), we investigated the conductivity of ZnSe layers that were implanted with F or Cl.

Table 1: Overview of the implanted ZnSe samples used for our studies. Sample A was implanted with three different implantation runs to obtain a homogeneous doping profile below the contacts. Samples B and C were implanted only once to reduce implantation damage. The ion energies and doses were adapted to achieve the same depth profile for both ion species.

sample	ion	energy (keV)	dose (cm^{-2})
A	F^-	110	4×10^{14}
		50	1×10^{14}
		20	6×10^{13}
B	F^-	20	2×10^{14}
C	Cl^-	40	1.2×10^{14}

We performed the ion implantation into ZnSe with varying implantation energies and doses as shown in Tab. 1. These implantation parameters were estimated on the basis of SRIM simulations: Firstly, we have chosen a maximum doping concentration of about $10^{19}\,cm^{-3}$ for comparison of all samples. Secondly, the implantation energy was adjusted to achieve the same penetration depth profiles for samples B and C. The latter were implanted with F and Cl, respectively, using only one implantation run. Furthermore, significantly low implantation energies were chosen to minimize implantation damage. Alternatively, in

sample A, Fluorine ions were implanted with three implantation runs with different energies and corresponding doses. These parameters allow to achieve a homogeneous doping profile in the order of $10^{19}\,\mathrm{cm}^{-3}$ within a region of $\sim 250\,\mathrm{nm}$ below the surface.

SRIM simulations (dashed lines) and quantified SIMS datasets (solid lines) of samples B and C are shown in Fig. 1. The SIMS profiles were obtained from the as-grown samples without any annealing treatment. Note that the depth profiles of both samples are nearly the same as we intended with the parameter sets obtained from the preceding SRIM simulations. Experimental and simulated ion concentrations are in good agreement especially close to the surface. However, the calculated penetration depth at which the concentration drops to $1/e$ of its maximal value is about 15 to 20 nm, while that measured by SIMS is larger (about 30 to 40 nm for both ion species) due to substantial ion channeling.

Electrical properties of contact and bulk material can be accessed experimentally when the total device resistance R is measured as a function of contact spacing L according to the TLM:[5,29,34]

$$R(L) = \rho_\mathrm{s} L/W + 2R_\mathrm{c} \tag{1}$$

The slope of $R(L)$ depends on the substrate sheet resistance ρ_s and the width W of the conducting channel. We assume both contacts to provide the same resistance R_c. For infinitely infinitesimally close contacts, R equals twice the contact resistance.

The electrical measurements for the samples listed in Tab. 1 are depicted in Fig. 2. The

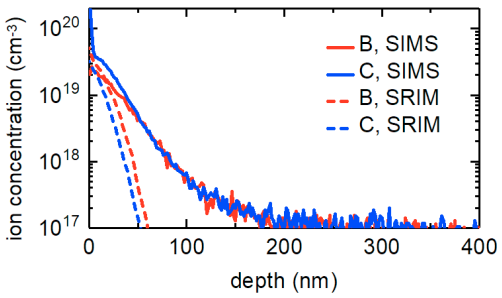

Figure 1: Quantified SIMS depth profiles (full curves) and corresponding SRIM simulations (dashed lines) of the ion concentration in the samples B and C.

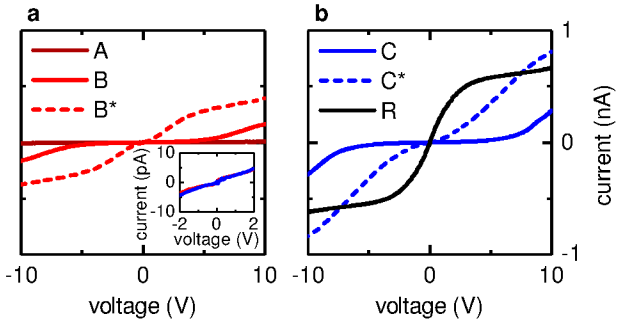

Figure 2: IV curves obtained from F and Cl implanted ZnSe samples. While different ion implantation parameters were used, all samples were measured with *in-situ* deposited Al contacts and 30 µm contact spacing. The asterisk marks annealed pieces of the samples. a) F implanted samples (A, B, B*). b) Cl implanted sample (C, C*) and undoped reference sample (R). The inset in a) represents an expanded view of the IV curves obtained from sample B and C for direct comparison at small voltages.

IV curves were achieved by two-terminal measurements at a needle probe station under ambient light conditions. Although we measured IV characteristics for several contact distances between 30 µm and 180 µm, no contact spacing dependent splitting of the curves was observed. The absence of such a dependence indicates a predominance of the contact resistance over the bulk resistance. For each of the implanted samples, the results obtained for $L = 30\,\mu\text{m}$ channel length are presented in Fig. 2. The common feature of the curves of all implanted samples is the high total resistance in the order of $10^{11}\,\Omega$ to $10^{12}\,\Omega$ especially at low voltages. Moreover, a severe nonlinearity of the IV curves in Fig. 2 is observed and reveals the presence of multiple current blocking regions below the contacts of all samples. Over the entire voltage range, the lowest current is measured in case of sample A which results from the severe implantation damage induced to this sample within the three implantation runs. A reduction of the implantation energy (sample B) distinctly increases the currents for voltages $> 5\,\text{V}$, however, the resistance around 0 V is only slightly decreased. The change from F to Cl ion implantation (sample C) further improves the IV characteristics at higher voltages, while the resistance around 0 V is similar to that of sample B. Although the Cl implantation was performed at higher acceleration voltages (Tab. 1), the conductivity of the samples is not further reduced. The latter indicates that Cl ions more efficiently compensate

the effect of implantation damage than F ions. However, for reference, we measured an undoped and unimplanted sample R, which exhibits a remarkably improved IV characteristics and an about two orders of magnitude reduced resistance of approximately $3 \times 10^9\,\Omega$ around 0 V. This demonstrates that the implantation damage on the atomic lattice exceeds the benefits of doping ZnSe by Cl and F implantation.

First-principles total-energy calculations performed by Laks et al.[27] suppose that Zn vacancies form acceptors in n-type ZnSe. Therefore, we conclude from the observed IV characteristics in Fig. 2 that our implantation technique leads to the formation of these Zn vacancies. The highest concentration of such defects is most likely located close to the surface, e.g. near the ZnSe/metal interface. Consequently, the p-like behaviour of the vacancies acts as a counterpart to the intended n-type doping. The samples B* and C* are pieces of the F and Cl implanted samples B and C that were thermally annealed for 3 min at 250 °C to recover the crystal structure and further activate donors. The corresponding IV curves shown as dashed lines in Fig. 2 indicate a reduction of the resistance within one order of magnitude in both cases. However, subsequent further annealing of samples B* and C* for additional 3 min at 300 °C induced a substantial degradation of the contacts and again an increase of the resistance (Fig. S1, Supporting Information).

Variation of contact metals and interface conditions of *in-situ* doped ZnSe:Cl

An alternative doping technique to ion implantation is *in-situ* doping of the ZnSe layer during MBE growth. As doping atoms, both F and Cl were studied. In case of F, doping concentrations in the order of $10^{19}\,\mathrm{cm}^{-3}$ were obtained but the incorporation of F drastically hindered the epitaxial growth of the ZnSe films. However, for Cl, successful epitaxial doping has already been reported.[25,28] We were able to control both, the layer thickness and Cl concentration and obtained doping levels up to $2 \times 10^{19}\,\mathrm{cm}^{-3}$ (Fig. S2, Supporting Information). In the following, we will use this ZnSe doping method for studying the metal contact

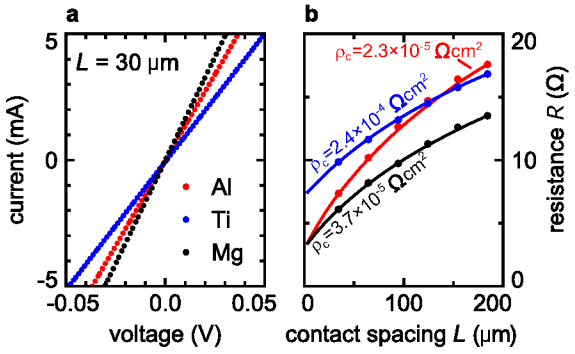

Figure 3: Metal contacts to n-type ZnSe fabricated by the *in-situ* method. a) IV data for different contact materials (Al, Ti, Mg) on separate ZnSe:Cl substrates ($n_{\mathrm{Cl}} \approx 10^{19}\,\mathrm{cm}^{-3}$). The lateral contact spacing is $L = 30\,\mu\mathrm{m}$. b) Total device resistance for Al, Ti and Mg as a function of the contact spacing L for samples without mesa etched linear transport channel (same color code as in panel a). Fits to the data are plotted with solid-lines and labeled with the fitted contact resistivities ρ_{c}.

resistivity ρ_c in this section. All samples provide a Cl concentration of $n_{\mathrm{Cl}} > 10^{19}\,\mathrm{cm}^{-3}$ which is on the metallic side of the MIT. In case of all *ex-situ* techniques contact formation at the metal-ZnSe interface is hampered due to formation of a native oxide. XPS studies performed in Ref. 35 identified this native oxide as a thin SeO_2 layer on top of the ZnSe surface. So far in the literature the lowest ρ_c was reported for a layer stack of Ti/Pt/Au contacts[5] where the oxide was wet-chemically removed prior to metallization. We also carried out several post-growth surface treatments (see Supporting Information), but none of them has led to a substantial improvement of the contact performance. Consequently, we focused our main efforts on entirely avoiding any oxide formation by making use of *in-situ* fabrication (e.g. maintaining UHV conditions between ZnSe MBE growth and the metallization step). Due to the low barrier height according to the Schottky model,[36] the contact metals Ti, Al and Mg were investigated in this study.

Fig. 3 a shows the IV characteristics for the *in-situ* deposited metal contacts with a distance of $L = 30\,\mu\mathrm{m}$. The data were obtained by four-terminal measurements in darkness at a needle probe station. For *in-situ* contacts, R is in the order of $10\,\Omega$ and the IV characteristic is linear in case of all three contact metals. Resistance variations between devices

with same metal contacts are less than 10 %. Furthermore, the device resistance shows a clear monotonic dependence on the contact spacing L (Fig. 3 b). We confirm the expectation of substantially lowered contact resistance for a metal-semiconductor interface without interfacial oxide by comparing *in-situ* and *ex-situ* (air exposure and various pre-treatments prior to metallization) contact resistivities (Fig. S3 and S4, Supporting Information).

We now quantify the contact resistivities of the *in-situ* metal contacts. Fig. 3 b shows a non-linear dependence of $R(L)$, since the samples do not provide a mesa etched linear transport channel. To include the fully three-dimensional nature of the current distribution in our device, we applied a finite-element solver and modeled the device with a Cl-doped ZnSe layer of thickness t, a 10 nm thin resistive contact interface layer and a perfect contact metal (neglecting metal resistance). $R(L)$ is fitted using the ZnSe bulk resistivity ρ_b and the metal/ZnSe contact resistivity ρ_c as free parameters (solid lines in Fig. 3 b). According to the TLM,[29] the current density under the metal contact drops on a length scale of the transfer length L_t

$$L_\mathrm{t} = \sqrt{\frac{\rho_\mathrm{c}}{\rho_\mathrm{s}}} \tag{2}$$

where $\rho_\mathrm{s} = \rho_\mathrm{b}/t$ is the ZnSe:Cl sheet resistance. The fits provide both ρ_s and L_t, from which ρ_c can be calculated using Eq. 2 (see Fig. 3 b). The simulated transfer lengths and sheet resistances are 7.7 µm, 11.4 µm, 29.5 µm and 39 Ω/sq, 29 Ω/sq, 27 Ω/sq for the contact metals Al, Mg and Ti, respectively. The lowest contact resistance at room temperature $\rho_\mathrm{c} = 2.3 \times 10^{-5}\,\Omega\mathrm{cm}^{-2}$ is determined for Al. The width of the metal contact (along the bias gradient) is larger than L_t by a factor of 6 at least, thus Eq. 2 applies. Remarkably, the contact resistances for Al and Mg of the samples fabricated with the *in-situ* method are well-below the value of $\rho_\mathrm{c} = 3.4 \times 10^{-4}\,\Omega\mathrm{cm}^2$ observed in Ref. 5. In this reference, wet chemical etching of the ZnSe after exposition to air was investigated. With our proposed *in-situ* method, we observed to our knowledge the best room temperature values regarding the contact resistivity of n-ZnSe contacts. In particular, the low Φ_m metals Al and Mg show excellent values for both L_t and ρ_c. This progress allows us to study the ohmic contact

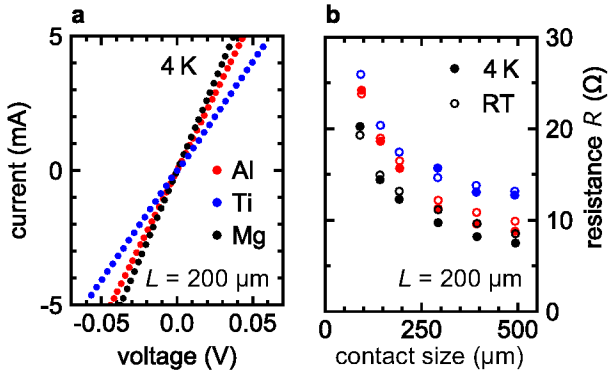

Figure 4: Properties of metal contacts to n-type ZnSe fabricated by the *in-situ* method. a) IV data measured at 4 K for different contact materials (Al, Ti, Mg) on ZnSe:Cl samples ($n_{\mathrm{Cl}} \approx 10^{19}\,\mathrm{cm}^{-3}$). The lateral contact spacing is $L = 200\,\mu\mathrm{m}$, contact size is 500 µm. b) Total device resistance as a function of the side length of square-shaped metal contacts for Al, Ti, and Mg (same color code as in panel a). R is measured at room temperature (open circles) and at 4 K (dots), respectively. Resistances of setup wiring are subtracted.

resistance at a temperature of 4 K.

Ohmic contacts to ZnSe operated at 4 K

Since all-electrical quantum devices such as EDQDs operate at low temperatures down to 10 mK, we study whether our ohmic contacts remain operable at 4 K. At this temperature thermionic charge transport across the Schottky or any other contact barrier is sufficiently suppressed. Fig. 4 a shows the IV characteristic of Al, Mg, and Ti ohmic contacts to ZnSe:Cl ($n_{\mathrm{Cl}} \approx 10^{19}\,\mathrm{cm}^{-3}$) measured at 4 K. Wire bonding is used to electrically contact the structures. (Using a 20 µm thick Al wire, typical wire-bond parameters are a bond power of 240 mW×40 ms = 0.96 mJ, which is adjusted to be as low as possible. We experienced insufficient adhesion applying Au ball bonding on the Al pads.) The data is corrected for resistances of the setup wiring by subtracting the separately measured temperature-dependent resistance offset of the setup or by using four-terminal measurements. We observe linear IV characteristics, the slopes of which are slightly dependent on the contact metal. Fig. 4 b shows the extracted resistances for each contact metal as a function of the side length of the contact pads. The observed super-linear drop of the device resistance is expected, as

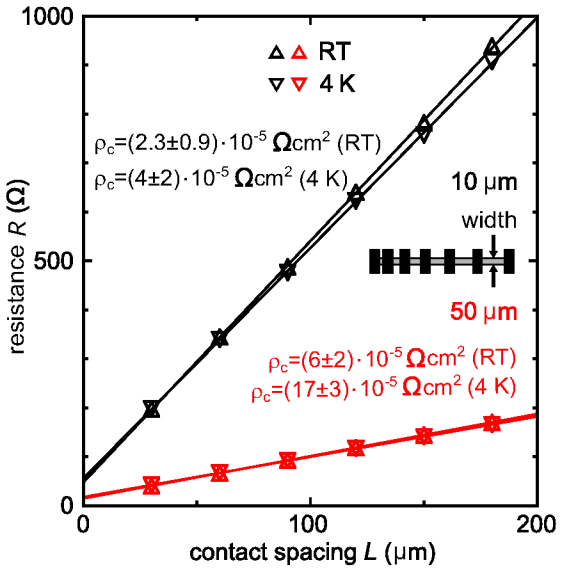

Figure 5: Characteristics of mesa devices with *in-situ* Al contacts at RT and 4 K. $R(L)$ for different channel widths gives direct access to bulk and contact resistivities that are similar for RT and 4 K. Simulations (lines) can reproduce the data by fitting ρ_c and ρ_s. Resulting ρ_c is given next to the data. The inset shows the device geometry used for definition of contacts (black) on a mesa etched doped ZnSe channel (black/gray).

the contact area increases quadratically with the contact size. Note that the resistances roughly coincide for 4 K and RT, since two effects, the bulk resistivity reduction (depending on electron mobility and bulk doping concentration) and the contact resistivity increase, seem to counterbalance. Most importantly, the contact resistance depends only marginally on temperature and we conclude that a thermionic part of charge transport across the metal/ZnSe junction is negligible.

The excellent performance observed for *in-situ* fabricated contacts enables us to quantitatively study contact resistance and transfer length of Al/ZnSe:Cl ohmic contacts at 4 K. We have chosen Al contacts as they provide low ρ_c and are easy to fabricate. Two mesa devices on a 10x10 mm^2 chip were characterized including error analysis. Typical fabrication tolerances in device dimensions of $\approx$ 1 µm for optical lithography and ZnSe layer thickness variations of 2 % across the chip enter the error calculations. Structures with two different channel widths (10 µm and 50 µm) are investigated. Fig. 5 shows the device resistance R for the 10 µm and the 50 µm mesa samples with varying contact spacing for both RT and

4 K. The linear increase in R with increasing contact spacing equivalent to the mesa channel length is clearly visible. Remarkably, no significant temperature dependence of R is observed. The small decrease of $\frac{\partial R}{\partial L}$ at 4 K compared to RT agrees with a small decrease of the bulk ZnSe resistivity observed by Hall measurements at 4 K.

For quantitative results a finite element solver and the device geometry is utilized to determine transfer length and contact resistivity. $R(L)$ is fitted using ZnSe bulk resistivity and contact resistivity as free parameters. Fig. 5 shows good agreement of measurement and simulation. Based on these considerations, for Al, the specific contact resistivity at room temperature is determined with $\rho_c = (2.3 \pm 0.9) \times 10^{-5}\,\Omega\mathrm{cm}^2$ ($L_t = (7 \pm 2)\,\mu\mathrm{m}$, $\rho_s = (44 \pm 3)\,\Omega/\mathrm{sq}$) for the 10 µm wide mesa device and $\rho_c = (6 \pm 2) \times 10^{-5}\,\Omega\mathrm{cm}^2$ ($L_t = (11 \pm 2)\,\mu\mathrm{m}$, $\rho_s = (45.5 \pm 0.7)\,\Omega/\mathrm{sq}$) for the 50 µm wide mesa device. At 4 K, the contact resistivity increases for both structures up to $\rho_c = (4 \pm 2) \times 10^{-5}\,\Omega\mathrm{cm}^2$ ($L_t = (10 \pm 2)\,\mu\mathrm{m}$, $\rho_s = (42 \pm 3)\,\Omega/\mathrm{sq}$) and $\rho_c = (17 \pm 3) \times 10^{-5}\,\Omega\mathrm{cm}^2$ ($L_t = (20 \pm 2)\,\mu\mathrm{m}$, $\rho_s = (42 \pm 3)\,\Omega/\mathrm{sq}$) for the 10 µm and the 50 µm structure, respectively.

Local ohmic contacts fabricated using a regrowth process

Following the above presented results of excellent ohmic contact performance with *in-situ* Al contacts on ZnSe:Cl substrates doped during MBE growth, we developed a regrowth fabrication process to demonstrate local ohmic contacts that are in principle suitable to access a buried conducting channel in a ZnSe based heterostructure selectively. For this approach, we used a ZnSe:Cl substrate with a carrier concentration of about $7.5 \times 10^{17}\,\mathrm{cm}^{-3}$. The sample was *in-situ* capped with Al_2O_3 as a mask to enable subsequent selective epitaxial overgrowth with highly doped ZnSe:Cl. Firstly, the sample was covered with the photoresist AZ 5214 E and via optical lithography, openings for the designated ohmic contacts were defined in the resist. Then the Al_2O_3 was removed in these holes using standard reactive ion etching (RIE) with a CHF_3/O_2 mixture (55 sccm/5 sccm), and subsequently we further etched about 35 nm deep into the ZnSe:Cl layer by RIE using a Cl_2/Ar mixture (50 sccm/5 sccm). To

remove potential near-surface defects that may have been caused by RIE and smoothen the ZnSe surface inside the hole, a wet chemical etching step with a $K_2Cr_2O_7$:HBr:H_2O solution was conducted. Afterwards, the sample was transferred into UVH conditions within 30 minutes. Before application of the epitaxial overgrowth, a thermal cleaning for 30 min at 150 ° C together with a hydrogen plasma cleaning for 5 min was conducted to remove contaminants and oxide on ZnSe.[37–39] Following this surface treatment, the sample was ramped up to a substrate temperature of about 290 °C while contineously providing a growth typical Zn flux (e.g. about 1×10^{-6} mbar beam equivalent pressure). Then, ZnSe:Cl with a doping concentration in the order of $10^{19}\,\mathrm{cm}^{-3}$ was epitaxially regrown by MBE to fill up the predefined holes. Finally, on top of the ZnSe:Cl, *in-situ* Al ohmic contacts were deposited and the redundant material between the contacts was etched away from the Al_2O_3 layer. The cross-section drawing of the obtained device structure is illustrated in Fig. 6 a.

Additionally, a reference sample was fabricated. The cross-section drawing of this sample is presented in Fig. 6 b. Hereby, we have grown another ZnSe:Cl substrate with same thickness and doping concentration as the regrowth sample. However, in this case, an additional about 30 nm thick ZnSe:Cl layer ("layer 2") with a doping concentration in the order of $10^{19}\,\mathrm{cm}^{-3}$ was grown on top of the substrate during the same MBE run. This configuration consequently provides the ideal interface between the substrate and the highly doped ZnSe:Cl contact layer. Subsequently, *in-situ* Al was deposited to form the ohmic contact in the same way as for the regrowth sample. Finally, both the Al and the highly doped ZnSe:Cl layer were etched away between the contacts to enforce the current transport through the interface between the lower doped ZnSe:Cl substrate ("layer 1") and the highly doped ZnSe:Cl regions ("layer 2") below the Al contacts.

The comparison of the IV characteristics of both samples allows to quantify the impact of the regrowth interface (i.e. between the etched ZnSe:Cl substrate surface and the regrown Al/ZnSe:Cl contact region) on the current transport. Fig. 6 c shows the IV characteristics of the regrowth (red) and the reference sample (black) at room temperature (full curves) and 4 K

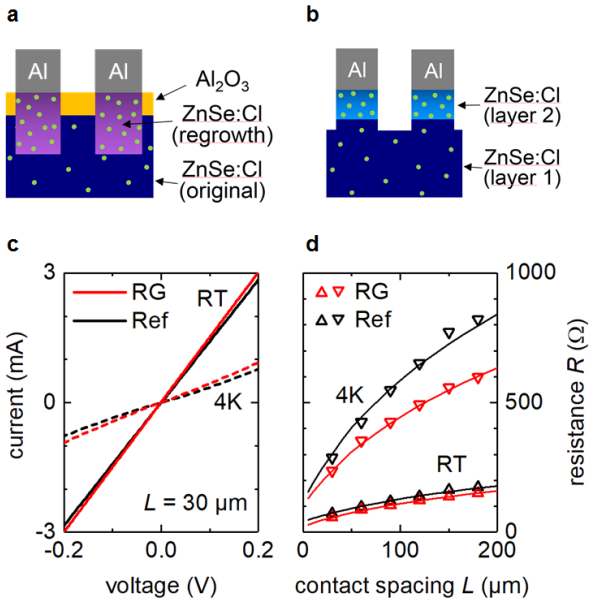

Figure 6: Local ohmic contacts on a sample fabricated via the regrowth method (RG) and a corresponding reference sample (Ref), both measured at room temperature and 4 K. a) Schematic cross-section view of the regrowth sample and b) of the reference sample, respectively. c) IV characteristics for both samples with an exemplary contact spacing of 30 µm. d) Total resistance (symbols) as a function of contact spacing and the related simulations (lines).

(dashed lines), respectively. Remarkably, the behavior is nearly identical for both samples. At room temperature, the curves are linear whereas they exhibit a slight non-linearity at 4 K. Fig. 6 d shows the total resistance of each sample as a function of the contact spacing. The contact resistivities are extracted from the related finite element simulations; $\rho_c(\mathrm{RG}) = (1.7 \pm 0.2) \times 10^{-4}\,\Omega\mathrm{cm}^{-2}$ and $\rho_c(\mathrm{Ref}) = (5 \pm 1) \times 10^{-4}\,\Omega\mathrm{cm}^{-2}$ at room temperature as well as $\rho_c(\mathrm{RG}) = (1.4 \pm 0.4) \times 10^{-3}\,\Omega\mathrm{cm}^{-2}$ and $\rho_c(\mathrm{Ref}) = (1.0 \pm 0.2) \times 10^{-3}\,\Omega\mathrm{cm}^{-2}$ at 4 K. We obtain similar results for the regrowth and the reference sample, which demonstrates the excellent quality of the regrowth interface and the absence of current transport barriers due to the etching and regrowth process. Furthermore, the resistances are distinctively increased at 4 K. Together with the non-linearity of the IV curves, we attribute this effect to the comparably low carrier concentration of the ZnSe:Cl substrate ($n_{\mathrm{Cl}} \approx 7.5 \times 10^{17}\,\mathrm{cm}^{-3}$), which is considerably below the carrier concentration of the MIT and therefore also temperature

dependent. This is consistent with the values obtained for the sheet resistances at 4 K ($\rho_s(\mathrm{RG}) = (1.8 \pm 0.2)\,\mathrm{k\Omega/sq}$ and $\rho_s(\mathrm{Ref}) = (2.0 \pm 0.2)\,\mathrm{k\Omega/sq}$), which are about a factor of 50 higher than the sheet resistances obtained for the highly doped ZnSe:Cl substrate in the previous section.

Conclusions

Low resistivity ohmic contacts to the wide-band-gap material ZnSe have been investigated. Hereby, we studied two different doping methods and fabrication techniques for the contact formation: F and Cl ion implantation led to strong irreversible implantation damage hindering the formation of ohmic contacts. Alternatively, epitaxial doping with Cl during MBE growth allows to control doping concentration and mobility. For substrates with doping concentration above the MIT, we identify *in-situ* deposited Al as the best contact metal to obtain low-resistivity ohmic contacts. The properties of these contacts were quantified by TLM, revealing contact resistivities as low as $\rho_c = 2.3 \times 10^{-5}\,\Omega\mathrm{cm}^2$ at RT and $\rho_c = 4 \times 10^{-5}\,\Omega\mathrm{cm}^2$ at 4 K, respectively, obtained from the best device.

Finally, we demonstrate that the *in-situ* contact method can be combined with a novel regrowth technique. The latter enables fabrication of local contacts to a buried conducting layer preserving the excellent properties of highly doped ZnSe:Cl samples with *in-situ* Al contacts at room temperature and 4 K. The comprehensive study of the ohmic contact performance on ZnSe:Cl using *in-situ* metal contact deposition in combination with the sophisticated regrowth technique for local ohmic contacts opens up enormous potential of ZnSe based heterostructures for application in novel all-electrical quantum devices operated at cryogenic temperature.

Acknowledgement

We gratefully acknowledge technical support by C. Krause and B. Bennemann on the sample MBE growth and fabrication support of the cleanroom staff at the Helmholtz Nano Facility (HNF) at Forschungszentrum Jülich. Furthermore, we thank U. Breuer from the Central Institute for Analytics (ZEA-3) for SIMS measurements and A. Dahmen from the Peter Grünberg Institute (PGI-9) for ion implantation.

This work was funded by the German Research Foundation (DFG) within the projects Nr. 337456818, Nr. 269990702 and the cluster of excellence "Matter and light for quantum computing" (ML4Q).

Supporting Information Available

- Post implantation annealing at 300 °C
- Doping of ZnSe with Chlorine during MBE growth (SIMS and Hall measurements)
- *IV* characteristics and resistances for different contact metals
- *IV* characteristics for Al contacts with and without Ar milling treatment

References

(1) Hayashida, K.; Nishio, M.; Mitsuishi, Y.; Guo, Q.; Ogawa, H. Growth of n-type ZnTe films and formation of ohmic contacts. Fourth International Conference on Thin Film Physics and Applications. 2000; pp 248 – 251.

(2) Ponpon, J. P. A review of ohmic and rectifying contacts on cadmium telluride. *Solid-State Electronics* **1985**, *28*, 689 – 706.

(3) Lukyanchikova, N. B.; Pekar, G. S.; Tkachenko, N. N.; Shin, H. M.; Sheinkman, M. K. Ohmic contacts to low-resistivity ZnS: Preparation, noise properties and nature of contact resistance. *Solid-State Electronics* **1977**, *20*, 879 – 882.

(4) Park, M. R.; Anderson, W. A.; Jeon, M.; Luo, H. Ohmic contacts to n-type and p-type ZnSe. *Solid-State Electronics* **1999**, *43*, 113–121.

(5) Miyajima, T.; Okuyama, H.; Akimoto, K. Ti / Pt / Au Ohmic Contacts to n-Type ZnSe. *Japanese Journal of Applied Physics* **1992**, *31*, 1743 – 1745.

(6) Knobel, R.; Samarth, N.; Crooker, S.; Awschalom, D. Spin-polarized quantum transport and magnetic field-dependent carrier density in magnetic two-dimensional electron gases. *Physica E: Low-dimensional Systems and Nanostructures* **2000**, *6*, 786–789.

(7) Berry, J. J.; Knobel, R.; Ray, O.; Peoples, W.; Samarth, N. Modulation-doped ZnSe/(Zn,Cd,Mn)Se quantum wells and superlattices. *Journal of Vacuum Science & Technology B: Microelectronics and Nanometer Structures Processing, Measurement, and Phenomena* **2000**, *18*, 1692.

(8) Hanson, R.; Kouwenhoven, L. P.; Petta, J. R.; Tarucha, S.; Vandersypen, L. M. K. Spins in few-electron quantum dots. *Reviews of Modern Physics* **2007**, *79*, 1217–1265.

(9) Zwanenburg, F. A.; Dzurak, A. S.; Morello, A.; Simmons, M. Y.; Hollenberg, L. C. L.; Klimeck, G.; Rogge, S.; Coppersmith, S. N.; Eriksson, M. A. Silicon quantum electronics. *Reviews of Modern Physics* **2013**, *85*, 961–1019.

(10) Fujita, T.; Kiyama, H.; Morimoto, K.; Teraoka, S.; Allison, G.; Ludwig, A.; Wieck, A. D.; Oiwa, A.; Tarucha, S. Nondestructive Real-Time Measurement of Charge and Spin Dynamics of Photoelectrons in a Double Quantum Dot. *Physical Review Letters* **2013**, *110*, 266803.

(11) Fujita, T.; Morimoto, K.; Kiyama, H.; Allison, G.; Larsson, M.; Ludwig, A.; Valentin, S. R.; Wieck, A. D.; Oiwa, A.; Tarucha, S. Single photoelectron spin detection and angular momentum transfer in a gate defined quantum dot. **2015**,

(12) Joecker, B.; Cerfontaine, P.; Haupt, F.; Schreiber, L. R.; Kardynał, B. E.; Bluhm, H. Transfer of a quantum state from a photonic qubit to a gate-defined quantum dot. *Physical Review B* **2019**, *99*, 205415.

(13) Bluhm, H.; Foletti, S.; Mahalu, D.; Umansky, V.; Yacoby, A. Enhancing the Coherence of a Spin Qubit by Operating it as a Feedback Loop That Controls its Nuclear Spin Bath. *Physical Review Letters* **2010**, *105*, 216803.

(14) Sleiter, D. J.; Sanaka, K.; Kim, Y. M.; Lischka, K.; Pawlis, A.; Yamamoto, Y. Optical Pumping of a Single Electron Spin Bound to a Fluorine Donor in a ZnSe Nanostructure. *Nano Letters* **2013**, *13*, 116–120.

(15) Lauck, R.; Schönherr, E. Isotopically pure ZnSe crystals grown from the vapor. *Journal of Crystal Growth* **1999**, *197*, 513–516.

(16) Pawlis, A.; Mussler, G.; Krause, C.; Bennemann, B.; Breuer, U.; Grützmacher, D. MBE Growth and Optical Properties of Isotopically Purified ZnSe Heterostructures. *ACS Applied Electronic Materials* **2019**, *1*, 44–50.

(17) Fowler, A. G.; Mariantoni, M.; Martinis, J. M.; Cleland, A. N. Surface codes: Towards practical large-scale quantum computation. *Physical Review A* **2012**, *86*, 032324.

(18) Pawlis, A.; Berstermann, T.; Brüggemann, C.; Bombeck, M.; Dunker, D.; Yakovlev, D. R.; Gippius, N. A.; Lischka, K.; Bayer, M. Exciton states in shallow ZnSe/(Zn,Mg)Se quantum wells: Interaction of confined and continuum electron and hole states. *Phys. Rev. B* **2011**, *83*, 115302.

(19) Hölscher, H. W.; Nöthe, A.; Uihlein, C. Investigation of band masses and g values of ZnSe by two-photon magnetoabsorption. *Physical Review B* **1985**, *31*, 2379–2387.

(20) Zajac, D. M.; Hazard, T. M.; Mi, X.; Nielsen, E.; Petta, J. R. Scalable Gate Architecture for a One-Dimensional Array of Semiconductor Spin Qubits. *Physical Review Applied* **2016**, *6*, 054013.

(21) Vandersypen, L. M. K.; Bluhm, H.; Clarke, J. S.; Dzurak, A. S.; Ishihara, R.; Morello, A.; Reilly, D. J.; Schreiber, L. R.; Veldhorst, M. Interfacing spin qubits in quantum dots and donors—hot, dense, and coherent. *npj Quantum Information* **2017**, *3*, 34.

(22) van der Wiel, W. G.; De Franceschi, S.; Elzerman, J. M.; Fujisawa, T.; Tarucha, S.; Kouwenhoven, L. P. Electron transport through double quantum dots. *Rev. Mod. Phys.* **2002**, *75*, 1–22.

(23) Huang, P.; Hu, X. Spin relaxation in a Si quantum dot due to spin-valley mixing. *Physical Review B* **2014**, *90*, 235315.

(24) Jones, G.; Woods, J. The electrical properties of zinc selenide. *Journal of Physics D: Applied Physics* **1976**, *9*, 799–810.

(25) Ohkawa, K.; Mitsuyu, T.; Yamazaki, O. Characteristics of Cl-doped ZnSe layers grown by molecular-beam epitaxy. *Journal of Applied Physics* **1987**, *62*, 3216–3221.

(26) Kuttler, M.; Strassburg, M.; Stier, O.; Pohl, U. W.; Bimberg, D.; Kurtz, E.; Nürnberger, J.; Landwehr, G.; Behringer, M.; Hommel, D. Doping dependent ZnCdSe/ZnSe-superlattice disordering. *Applied Physics Letters* **1997**, *71*, 243–245.

(27) Laks, D. B.; Van de Walle, C. G.; Neumark, G. F.; Blöchl, P. E.; Pantelides, S. T. Native defects and self-compensation in ZnSe. *Physical Review B* **1992**, *45*, 10965–10978.

(28) Karczewski, G.; Hu, B.; Yin, A.; Luo, H.; Furdyna, J. K. Deep electron states in chlorine-doped ZnSe films grown by molecular beam epitaxy. *Journal of Applied Physics* **1994**, *75*, 7382–7388.

(29) Berger, H. Models for contacts to planar devices. *Solid-State Electronics* **1972**, *15*, 145–158.

(30) Dennard, R.; Gaensslen, F.; Rideout, V.; Bassous, E.; LeBlanc, A. Design of ion-implanted MOSFET's with very small physical dimensions. *IEEE Journal of Solid-State Circuits* **1974**, *9*, 256–268.

(31) Haijiang Yu,; McCarthy, L.; Rajan, S.; Keller, S.; Denbaars, S.; Speck, J.; Mishra, U. Ion implanted AlGaN-GaN HEMTs with nonalloyed Ohmic contacts. *IEEE Electron Device Letters* **2005**, *26*, 283–285.

(32) Mozzi, R. L.; Fabian, W.; Piekarski, F. J. Nonalloyed Ohmic contacts to n-GaAs by pulse-electron-beam-annealed selenium implants. *Applied Physics Letters* **1979**, *35*, 337–339.

(33) Kamata, A.; Uemoto, T.; Okajima, M.; Hirahara, K.; Kawachi, M.; Beppu, T. Superiority of group VII elements over group III elements as donor dopants in MOCVD ZnSe. *Journal of Crystal Growth* **1988**, *86*, 285–289.

(34) Ting, C.-Y.; Chen, C. Y. A study of the contacts of a diffused resistor. *Solid-State Electronics* **1971**, *14*, 433–438.

(35) Schüll, K.; Spahn, W.; Hock, V.; Lunz, U.; Ehinger, M.; Faschinger, W.; Landwehr, G. Non-metal in situ and ex situ ohmic contacts to n-ZnSe. *Semiconductor Science and Technology* **1997**, *12*, 485–489.

(36) Sze, S. M. *Semiconductor Devices: Physics and Technology*; John Wiley & Sons Singapore Pte. Limited, 2012.

(37) Ohno, T.; Ohki, A.; Matsuoka, T. Surface cleaning with hydrogen plasma for low-defect-density ZnSe homoepitaxial growth. *Journal of Vacuum Science & Technology A* **1998**, *16*, 2539–2545.

(38) Hughes, W.; Boney, C.; Johnson, M.; Cook, J.; Schetzina, J. Surface preparation of ZnSe substrates for MBE growth of II–VI light emitters. *Journal of Crystal Growth* **1997**, *175-176*, 546 – 551.

(39) Sasaki, Y.; Ohashi, M.; Tsubono, I.; Kimura, N.; Sawada, T.; Suzuki, K.; Imai, K.; Saito, H. Cleaning effect of ZnSe surface by hydrogen treatment. *physica status solidi (c)* **2004**, *1*, 670–673.

Graphical TOC Entry